

# Extending h adaptivity with refinement patterns

Giovane Avancini<sup>a</sup>, Nathan Shauer<sup>a</sup>, Francisco T. Orlandini<sup>a</sup>, Paulo Cesar A. Lucci<sup>b</sup>, Philippe R. B. Devloo<sup>a</sup>

<sup>a</sup>Universidade Estadual de Campinas, R. Josiah Willard Gibbs 85 - Cidade Universitaria, Campinas SP, Brazil, CEP 13083-839

<sup>b</sup>Exact Sciences, Environmental and Technologies Center, Pontifical Catholic University of Campinas (PUC-Campinas), Campinas 13086-099, Brazil

---

## Abstract

This contribution introduces the idea of refinement patterns for the generation of optimal meshes in the context of the Finite Element Method. The main idea is to generate a library of possible patterns on which elements can be refined and use this library to inform an h adaptive code on how to handle complex refinements in regions of interest. There are no restrictions on the type of elements that can be refined, and the patterns can be generated for any element type. The main advantage of this approach is that it allows for the generation of optimal meshes in a systematic way where, even if a certain pattern is not available, it can easily be included through a simple text file with nodes and sub-elements. The contribution presents a detailed methodology for incorporating refinement patterns into h adaptive Finite Element Method codes and demonstrates the effectiveness of the approach through mesh refinement of problems with complex geometries.

*Keywords:* Finite Element Method; Refinement Patterns; Mesh Generation; Adaptive Mesh Refinement; Hanging Nodes.

---

## 1. Introduction

The Finite Element Method (FEM) is a powerful numerical technique widely used in various fields of engineering and science for solving partial differential equations. One of the key advantages of the FEM is its ability to handle complex geometries and adaptively refine the mesh to accurately capture the solution behavior in regions of interest. In particular, adaptive h-p refinement, which combines both mesh refinement (h-refinement) and polynomial degree refinement (p-refinement), has been proven to be highly effective in achieving accurate and efficient solutions [1, 2].

Overall, h-refinement combined with adaptive algorithms can play a crucial role in improving the accuracy of the solution by refining the mesh in regions of interest, especially in regions with strong gradients, boundary layers, and singularities [3]. Optimal mesh refinements for specific problems have been studied in the literature [4].

In the context of h-refinement, the generation of hanging nodes is a common issue that arises when refining the mesh towards a region of interest. The meshes created in this way are often called 1-irregular meshes. Hanging nodes occur when a refined element shares a face with a coarser element, resulting in a discontinuity in the solution across the interface that needs to be treated. Methodologies to do so have been proposed in the literature with an increased interest during the 80s and 90s. The most common approach is to impose the continuity between elements as a restriction to the shape functions of both elements at a given interface [5–8]. This methodology has been implemented in the NeoPZ library [9] for 1D, 2D, and 3D elements of any polynomial order. Other methodologies have also been explored in the literature as for instance in [10] where transition elements are proposed that do not rely on constraints to produce interelement continuity. Recently, there has been renewed interest

---

*Email addresses:* [giovanea@unicamp.br](mailto:giovanea@unicamp.br) (Giovane Avancini), [shauer@unicamp.br](mailto:shauer@unicamp.br) (Nathan Shauer), [francisco.orlandini@gmail.com](mailto:francisco.orlandini@gmail.com) (Francisco T. Orlandini), [cesar.lucci@mac.com](mailto:cesar.lucci@mac.com) (Paulo Cesar A. Lucci), [phil@unicamp.br](mailto:phil@unicamp.br) (Philippe R. B. Devloo)

in the topic, for instance in [11–15] where new approaches to handle hanging nodes are proposed. In [12], the methodology is explored in the context of the Extended Finite Element Method (G/XFEM), and in [14] the authors propose a new approach to handle hanging nodes in the context of the Scaled Boundary Finite Element Method (SBFEM). It is important to note that methodologies to refine the mesh while avoiding the creation of hanging nodes have been proposed in the literature, as for instance in [16–20]. The refinement patterns proposed in this chapter are an efficient alternative that can be used to refine meshes in optimal ways. The concept of refinement patterns has been used with different objectives as in [21], where they are associated with transition meshes between coarse and fine regions of a finite element mesh.

In this contribution, we focus on extending h adaptivity with refinement patterns. Refinement patterns are a powerful tool that provides a systematic way to handle complex refinements in regions of interest. The main idea is to generate a library of possible patterns on which elements can be refined and use this library to inform an h adaptive code on how to tackle complex cases. It is noted that even if a refinement pattern does not exist apriori, it can be readily generated given the nodes and sub-elements that compose a certain refinement pattern. Refinement patterns can be used to refine meshes in optimal directions as explained in Section 4. By integrating refinement patterns into an h adaptivity framework, one can improve the overall solution quality and computational efficiency. The methodology here explained has been integrated into the NeopZ object-oriented environment for Finite Element (FE) analyses [9] and its implementation is used throughout the text to exemplify a possible way to integrate refinement patterns into an existing FE code.

The main contributions in this chapter are the following:

- The concept of refinement patterns and their role in addressing hanging nodes in adaptive h-refinement are introduced.
- A detailed methodology for incorporating refinement patterns into the Finite Element Method is presented.
- The generality of the proposed approach is illustrated through mesh refinement of problems with complex geometries.

In this contribution, we intentionally do not include simulation results related to the application of refinement patterns. Our main objective is to present the methodology and concept behind it, rather than focusing on specific simulations.

This chapter is organized as follows. Sections 2 and 3 provide an overview of the fundamental concepts of refinement patterns and implementation aspects. Section 4 presents necessary operations for the use of refinement patterns. Section 5 describes the methodology to generate a refinement pattern entry in the NeopZ library. Section 6 presents complex refinement cases and discussions. Finally, Section 7 concludes the chapter and the outlines for future research directions are presented in Section 8.

## 2. Mathematical description

The description of refinement patterns is based on the mathematical concept of parametrization of the master elements and their sides. These parametric spaces allow the formal description of the projection of points from the interior of an element to the sides of the element and vice-versa. They also allow to transfer point on an element/side to a corresponding point on its ancestor/side. Finally, the transformation between parametric spaces allows to formally describe shape function restraints for  $H^1$ ,  $H(\text{div})$  or  $H(\text{curl})$  spaces.

### 2.1. Affine transformations

An affine transformation  $T : R^n \rightarrow R^m$  has the form

$$\begin{aligned} x_m &= T(x_n) \\ &= A^{mn}x_n + B^m, \end{aligned}$$

where  $A^{mn}$  is an  $m \times n$  matrix and  $B^m$  an  $m$ -dimensional vector. Affine transformations are utilized to describe the relationship between parametric spaces of different entities in a finite element mesh.

A projection  $P : R^n \rightarrow R^n$  is an affine transformation such that

$$P(x_n) = P(P(x_n)).$$

When  $m = 3$  and  $n = 3$ , affine transformations describe graphical transformations commonly used in computer graphics. These transformations are so important that they motivated the creation of the graphical processor unit (GPU) [23].

## 2.2. Element topology

The element topology defines the parametric space associated with a master element. Table 1 enumerates the element topologies included in the NeoPZ environment. As mentioned in Section 1, the NeoPZ environment is implemented within an object-oriented paradigm and, therefore, concepts can be "encapsulated" with the use of classes. In this context, a `class` is dedicated to each topology available in the environment.

Each master element can be viewed as the union of open sets of points associated with sides. Each side is in turn associated with a topology and has an associated parametric space. The definition of the sides and their orientation is an integral part of the definition of the topology. Figure 1 illustrates the master element of a triangle. Note that the triangle is composed of 3 points (zero-dimensional sides), 3 edges (one-dimensional sides) and one face (two-dimensional side). An affine transformation can be defined between the parametric spaces associated with the sides and the master element space.

### Definitions

The following definitions are used in the description of the topology

- $T_{es}$ : Affine transformation that projects a point from the interior of the element to the parametric space of side  $s$ .
- $T_{se}$ : Affine transformation transforming the location of a point defined in a parametric space of side  $s$  to a point in the element space.

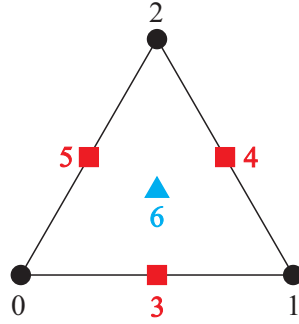


Figure 1: Topology of a triangular element composed of seven sides: three zero-dimensional sides (points) with local indices 0, 1, and 2; three one-dimensional sides (edges) with local indices 3, 4 and 5; and one two-dimensional side (face) with local index 6.

### Consistency checks

If a point  $x$  is such that it lies on a side then, there exists a point in parametric space of  $s$ , denoted  $x_s$ , such that

$$x = T_{se}x_s.$$

Also, if  $T_{es}$  projects a point in the element space onto a side and assuming that  $x$  lies on the side, then

$$x_s = T_{es}x,$$



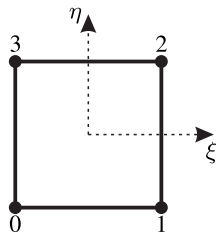
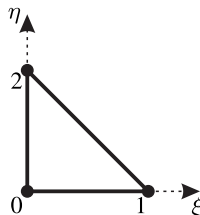
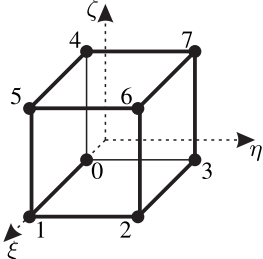
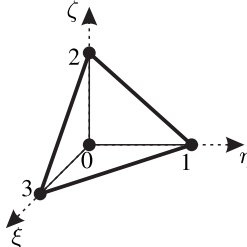
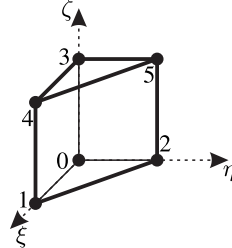
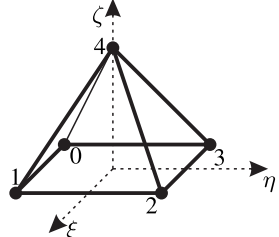
Name	Graphical representation	Parametric coordinates	Number of sides	Class name
Point		$\emptyset$	1	TPZPoint
Line		$-1 \leq \xi \leq 1$	3	TPZLine
Quadrilateral		$-1 \leq \xi \leq 1, -1 \leq \eta \leq 1$	9	TPZQuadrilateral
Triangle		$0 \leq \xi \leq 1, 0 \leq \eta \leq 1 - \xi$	7	TPZTriangle
Hexahedra		$-1 \leq \xi \leq 1, -1 \leq \eta \leq 1, -1 \leq \zeta \leq 1$	27	TPZCube
Tetrahedra		$0 \leq \xi \leq 1, 0 \leq \eta \leq 1 - \xi, 0 \leq \zeta \leq 1 - \xi - \eta$	15	TPZTetrahedron
Prism		$0 \leq \xi \leq 1, 0 \leq \eta \leq 1 - \xi, -1 \leq \zeta \leq 1$	21	TPZPrism
Pyramid		$-1 + \zeta \leq \xi \leq 1 - \zeta, -1 + \zeta \leq \eta \leq 1 - \zeta, 0 \leq \zeta \leq 1$	19	TPZPyramid

Table 1: Element topologies in local (or master) coordinate system.



implying that

$$x_s = T_{es}T_{se}x_s \quad \forall x_s.$$

Therefore, taking the composition of transforming a point in the parametric space of a side  $s$  to the element space and transforming it back to the side results in an identity operator (which is in fact a projection)

$$I_s = T_{es}T_{se}.$$

Defining the affine transformation  $P_s$  as the composition:

$$P_s = T_{es}T_{se},$$

then  $P_s$  is a projection operator such that

$$P_s P_s \equiv P_s.$$

Then clearly

$$\begin{aligned} P_s P_s &= T_{es}T_{se}T_{es}T_{se} \\ &= T_{es}I_sT_{se} \\ &= P_s, \end{aligned}$$

meaning that if a point from the element space is projected to the parametric space of a side and then back to element space, then this is in fact a projection.

#### *Composition of projections*

If the closure of a face  $f_a$  of a three-dimensional element contains the one-dimensional side  $s_c$  then the composition of the projection to the face  $P_{f_a}$  and the projection to side  $s_c$  (i.e.  $P_{s_c}$ ) is equal to the projection to  $s_c$

$$P_{s_c} = P_{s_c}P_{f_a}.$$

The description of the topology is the common denominator that relates the description of the geometry, the definition of the approximation space, and the definition of a numerical integration rule.

Each master element defines its own set of sides and orientations. In the **NeopZ** library the element topologies are defined in the **Topology** subdirectory of the library. Each topology **class** is **static**, meaning its behavior does not depend on an internal data structure. The parametric transformations between sides for the different topologies are documented in [24].

#### *2.3. Neighboring information*

The concept of viewing the master element as the union of open sets of points allows to define the concept of neighbors. Let  $A$  and  $B$  be two elements of a finite element mesh and  $S_A$  and  $S_B$  sides of these two elements. Then, element  $A$  is the neighbor of element  $B$  through side  $S_A$  if and only if the set of points associated with  $A/S_A$  is equal to the set of points associated with  $B/S_B$ . Figure 2 illustrates the concept of neighbors graphically.

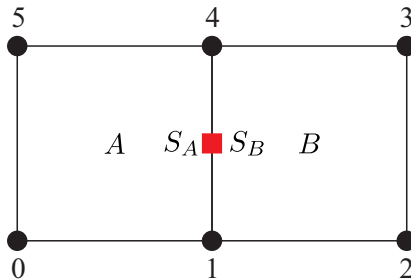


Figure 2: Illustration of two neighboring elements through the side with global node indices 1 and 4.

An element  $A$  along the side  $S_A$  can be a neighbor to more than one element/side. Dynamic memory allocation is avoided by keeping track of element neighbors in a circular structure. Figure 3 illustrates a point that is shared by 4 elements. The circular data structure represents a linked list:

$$A/S_A \rightarrow B/S_B \rightarrow C/S_C \rightarrow D/S_D \rightarrow A/S_A$$

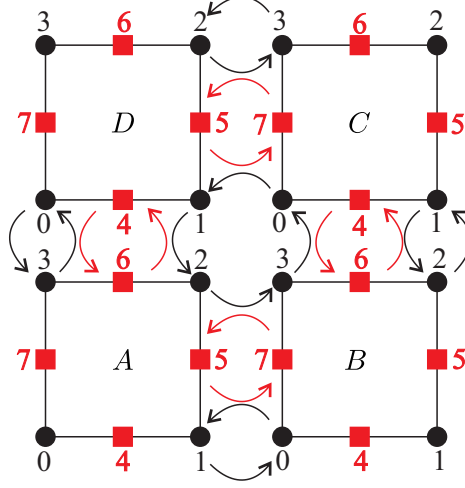


Figure 3: Circular data structure of neighboring elements. Black represents neighboring data structures between nodes and red represents neighboring data structures between edges.

As such the data structure associated with side  $S_A$  of element  $A$  only keeps track of element  $B/S_B$ . By cycling through the neighboring information of the element/sides, one can collect the complete set of elements/neighbors. As the number of sides of  $A$  is fixed (associated with the topology), a fixed-sized data structure keeps track of the neighboring information.

#### Building the neighboring information

Considering that the data structure of neighboring information is not standard, we describe a simple algorithm to build the neighboring information based on a *traditional* element node data structure.

The first premise is that each side of an element can be associated with a set of nodes. The closure of the side contains a given number of nodes. The global index of these nodes forms the set of nodes associated with a side.

The second premise is that, in a traditional finite element mesh, two elements are neighbors along one side if they share the associated set of nodes, *i.e.* the side is uniquely determined by the nodes (*e.g.* if two triangular sides share three nodes, then they are neighbors along a face).

#### A Neighbors along nodes

The first step is to loop over the elements once to fill in the neighboring information along the nodes. To do so, a temporary vector consisting of pairs of integers of the size of the number of nodes in the mesh is created. This data structure is denoted **NeighInfo** and will contain at each position one possible (element index)/(side index) pair associated with the global index of a node. Then the algorithm to fill in the neighboring information along nodes is shown in Algorithm 1.

#### B Neighbors along higher dimensional sides

Let **NeighSideInfo** be a temporary data structure created for each side of an element of size equal to the number of nodes of that side. Each position in **NeighSideInfo** pertains to a certain node of the side and will contain a set of integers of all the neighboring elements through that node. Note that the node neighboring data structure for each element has been previously computed in Algorithm 1. Algorithm 2 is used to compute all element neighbors through sides of dimension higher than 0.

It is noted that the complexity of this algorithm is linear. It can possibly be parallelized.

**Input:** Finite element mesh and **NeighInfo**

```

for Element  $e^i$  in the Finite Element Mesh do
  for Node  $n^j$  of  $e^i$  do
    if Position  $k$  of NeighInfo is not initialized where  $k$  is the global index of  $n^j$  then
      | Insert the pair  $e^i/n^j$  in position  $k$  of NeighInfo
    end
    else
      |  $e_i/n_j$  is inserted in the neighboring data structure of the element contained in
      | position  $k$  of NeighInfo
    end
  end
end

```

**Algorithm 1:** Algorithm to compute all element neighbors through nodes.

**Input:** Finite Element mesh

```

for Element  $e^i$  in the Finite Element Mesh do
  for Side  $s^j$  of  $e^i$  do
    if dimension of  $s^j$  is 0 then
      | continue
    end
    Create NeighSideInfo of size equal to the number of nodes of  $s^j$ 
    Fill NeighSideInfo based on data structure of neighboring nodes created using
    Algorithm 1
    Perform intersection of the sets in NeighSideInfo
    The result is the list of elements that are neighbors of  $e^i$  through side  $s^j$ 
  end
end

```

**Algorithm 2:** Algorithm to compute all element neighbors through sides of dimension higher than 0.

#### 2.4. Parametric transform between neighbors

Two elements are neighbors if they share a side. The parametric transform between both elements depends on the relative orientation of both sides. The number of possible combinations depends on the topology of the side. A line has two possible orientations, a triangle has six possible orientations, and a quadrilateral has eight possible orientations.

The correctness of the parametric transformation can be verified by the following tests: for an arbitrary point on side  $S_A$  of element  $A$ . The corresponding point on side  $S_B$  of element  $B$  is computed by the transformation  $T_{AB}$ . The  $x$  coordinate computed by element  $A$  should correspond to the  $x$  coordinate computed by element  $B$ .

#### 2.5. Parametric transform between son side and father side

It is an essential feature of geometric refinements that a *father* element is partitioned by its son elements. Moreover, each side of the son elements is entirely contained in a side of the father element. As a consequence of this property, an affine transformation can be defined between the parametric space of the son/side and the corresponding father/side. This affine transformation is computed by an  $L^2$  projection. Let  $A^{mn}$  and  $B^m$  be the matrix and vector of the affine transformation, respectively. The matrix  $A^{mn}$  and vector  $B^m$  are computed by minimizing the following functional:

$$\min_{A^{mn}, B^m} \int_{\hat{S}} \|x_S(\xi) - x_F(A^{mn}\xi - B^m)\|^2 d\xi, \quad (1)$$

where  $\hat{S}$  is the parametric space of the son/side,  $x_S$  is the cartesian coordinate of the son/side, and  $x_F$  is the cartesian coordinate of the father/side. In Section 3.3.2, the same functional is used to compute the affine transformation between the parametric space of the father element and the parametric space of the son element within the context of the **NeoPZ** environment.

### 3. Data structure and implementation aspects

In the following subsections, details regarding a choice of implementation of refinement patterns in the NeoPZ library [9] are discussed. In Subsection 3.1, preliminary concepts are introduced. Subsection 3.2 describes the data structure required for defining a valid refinement pattern and Subsection 3.3 discusses the operations to load refinement patterns into an FE code. Finally, in subsection 4, useful routines are presented in a *bottom-up* fashion, illustrating the building blocks needed to define the routine `RefineDirectional` and providing insights on the types of operations possible using these patterns. For more details on the implementation, the reader is referred to the classes `TPZRefPattern` and `TPZRefPatternTools` in the NeoPZ library available on [Github](#).

#### 3.1. Fundamental concepts of refinement patterns

The term refinement pattern is used here for describing a systematic way of geometrically refining an element, *i.e.*, splitting it into more elements. This procedure is performed in the reference (or master) element and, therefore, a given refinement pattern can be readily applied to different elements of the same type. In a given mesh, each element may also have refinement patterns associated with it because of *compatibility* with the refinement patterns of its neighboring elements. This means that the vertices created by the refinement pattern of one element must be compatible with the vertices created by the refinement pattern of its neighbors.

In practice, to reduce the number of needed refinement patterns, one idea is to use the concept of *permutation* of refinement patterns: since the refinement pattern is defined in the reference element, changing the node ordering of such element will result in different patterns. Being able to compute the permutations of a refinement pattern allows one to apply them to elements with a different node ordering.

It is noted that dividing an element into subelements using refinement patterns can either improve or worsen the aspect ratio of the original element. Using refinement patterns neither ensures nor impedes the improvement of the mesh quality.

#### 3.2. File structure defining a refinement pattern

A refinement pattern is described through a secondary geometric mesh – different than the finite element geometric mesh used for the simulation – whose domain  $\Omega$  corresponds to a given supported element type (linear, triangular, quadrilateral, hexahedral, *etc.*). It can thus be described in text format as in Figure 4.

Figure 4 illustrates a tetrahedron split into another tetrahedron and a wedge. The data file is divided into three sections. In the first section, we specify the number of nodes (7), the number of elements (3, including the original element that is refined), and provide both a numerical identifier and a name that are associated with the pattern. The second section consists of the numerical coordinates of the nodes in the three-dimensional domain. The third section specifies all the elements in the mesh, possibly assigning different identifiers for them. The first element to be described is always the father element and the subsequent 4 are the children. In this example, the tetrahedral (hexahedral) element is represented by the integer 4 (6), and all the elements are assigned the same identifier (`mat id`), 1.

Once a given refinement pattern is read using the file described in this section, the next step is to load it into the memory and use it to perform the necessary operations for applying this pattern to refine an element.

#### 3.3. Creating a refinement pattern

As discussed in the previous section, a refinement pattern consists of a secondary geometric mesh corresponding to a partition of a master element  $K$ . In this section, the procedures performed on this secondary mesh to apply a refinement pattern to a given element are discussed.

```

% int(# nodes) int(# elements)
7 3
% int(id) string(name)
-50 TetraDir1Side

% double[3](node coords)
0 0 0
1 0 0
0 1 0
0 0 1
0 0 0.5
0.5 0 0.5
0 0.5 0.5

% int(el type) int(mat id) int(node ids)
4 1 0 1 2 3
6 1 0 1 2 4 5 6
4 1 4 5 6 3

```

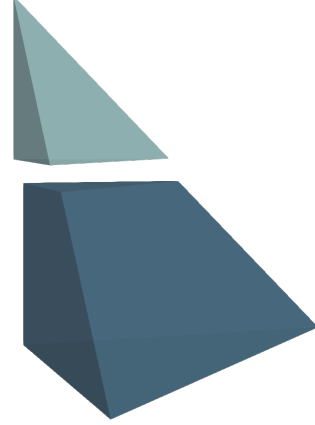


Figure 4: Description of a simple refinement pattern on a tetrahedron and the resulting elements.

### 3.3.1. Reading the pattern

Once this secondary geometric mesh is read, the first operation is to convert the coordinates of the nodes in  $K$  to the ones in  $\hat{K}$ , the *reference element*. If the original coordinates do not correspond to the coordinates of the master element, the inverse of the map  $F : \hat{K} \rightarrow K$  is used. This is important since refinement patterns are invariant under affine transformations.

Next, the usual connectivities of the mesh are computed, as described in Section 2.3. Then, the transformation between the possible *permutations* of the element is computed, as described in Subsection 3.1. By doing so, the pattern is available regardless of the node ordering of the element in the mesh. After these procedures, refinement-specific tasks have to be performed.

### 3.3.2. Sub-element parametric transformations

To obtain conforming approximation spaces, each sub-element in the refinement pattern must be aware of its relationship with the parent element so that the relevant traces of basis functions can be compatibilized. More specifically, each side of each sub-element needs to know which side in the parent element contains it and what is the parametric transformation to that side in the parent element in parametric coordinates.

**Input:** sub-elements  $K^e$  and parent element  $K^f$

```

for sub-element  $K^e \in \{K\}$  do
  for side  $s^e \in \partial K^e$  do
    Compute center of side  $s^e$  in  $\xi_f$  in the parametric coordinates of  $K^f$ 
    Find which side  $s^f$  of the father contains the center point of  $s^e$ 
    Compute the affine transformation  $F_e^f : \xi_{s^e} \rightarrow \xi_{s^f}$ 
    Store  $(s^f, F_e^f)$ 
  end
end

```

**Algorithm 3:** Computing parametric transform from the sides of the sub-elements to the side of the father element.

The transformation  $F_e^f$ , mapping a point in the parametric coordinates of the sub-element side  $s^e$  to a point in the parametric coordinates of the parent element's side  $s^f$  is computed by a minimization procedure. Namely, we search for the affine transform  $F_e^f : A\xi_{s^e} + B$  by finding the coefficients of  $A$  and  $B$  that minimize

$$\|\Delta\|^2 = \int_{\Omega_{se}} (\xi_{sf} - (A\xi_{se} + B)) \cdot (\xi_{sf} - (A\xi_{se} + B)) d\xi_{se}. \quad (2)$$

It is worth noting that the resulting  $F_e^f$  is exact only if the jacobian of the mapping of the sub-element is constant.

### 3.3.3. Parent element side partitioning

For each side of the father element, we store its *partition*. By partition, we mean a data structure containing:

- Indices of internal nodes that result from the refinement pattern that is contained in it.
- List of pairs of sub-element/side contained in it.

The partition of sides is used to compatibilize refinement patterns. This procedure can be better explained with an example. Assume that an element in a given mesh needs to be refined with a certain refinement pattern. Depending on the refinement pattern, new nodes are created in the mesh, that are contained in sides of the original element. The proposed paradigm dictates that these nodes should match nodes created on the corresponding side of a previously refined neighboring element, *i.e.*, their side-refinement patterns should be compatible (Side refinement patterns are the subject of the next section). However, this verification can be costly. Storing the partition can be used to check that a given pattern is not compatible significantly faster.

This algorithm can be easily computed with the data from Subsection 3.3.2, so it is omitted.

### 3.3.4. Side refinement patterns

A refinement pattern of an element implicitly defines refinement patterns for its sides. The refinement pattern of a side is defined by the refinement pattern of the element and the parametric transformation between the side and the element. When a neighboring element is refined, the refinement patterns associated with the neighboring sides should be identical. In other words, two neighboring elements have compatible refinement patterns if they have the same refinement pattern associated with their common side.

Embedded in a refinement pattern are the refinement patterns associated with each side of the element<sup>1</sup>, and they are used in operations associated with boundaries and interfaces between elements.

The creation of the side refinement patterns is performed recursively: the mesh associated with the side is created and its pattern is initialized (if not found in a database of previously loaded refinement patterns, as discussed in Section 5).

When a refinement pattern is applied to an element, the *code* checks whether the neighboring elements have compatible side refinement patterns. If they do not, the code will flag an error and abort. To assist the user in using the library, the code will also provide a list of compatible refinement patterns.

## 4. Refinement pattern tools

With the extension of the NeoPZ library to include refinement patterns, a set of tools is necessary to perform operations on these patterns: whereas refinements using uniform refinement patterns are always compatible, this is not the case when using general refinement patterns. The tools presented in this section are used to verify the compatibility of refinement patterns and to find compatible refinement patterns that match certain criteria.

---

<sup>1</sup>Except, obviously, for zero-dimensional sides.

#### 4.1. RefPatternEquality

Two refinement patterns are said to be equal if, and only if:

- For each element type, the same number of elements is present in both patterns
- The number of nodes in both patterns is the same
- There is a bijection between the nodes on both patterns
- Every sub-element has the same (mapped) nodes

#### 4.2. GetCompatibleRefPatterns

The refinement patterns are said to be compatible if, for every neighbor with a refined side, the element's side is refined exactly the same way. That implies that if no neighbors are refined, every refinement pattern is said to be compatible. Thus, compatibility refers to the fact that applying a given pattern on a certain element in a mesh will result in a conforming mesh. This procedure is described in Algorithm 4.

```

Input: element  $K_e$ 
for side  $s^i \in \partial K_e$  such that  $\dim s^i > 0$  do
  for neighbor  $K_n$  of  $(K, s^i)$  do
    if There is side  $s^n$  of  $K_n$  that is refined then
      Store refinement pattern2 of neighbors  $P_n^{s^i}$ 
    break
  end
end
end
for candidate pattern  $P$  of  $K_e$  do
  for side  $s^i \in \partial K_e$  such that  $\dim s^i > 0$  do
    if  $P_n^{s^i}$  exists then
      if side pattern of  $P$  is different from  $P_n^{s^i}$  then
        Mark as non-compatible
      break
    end
  end
end
if  $P$  is not marked as non-compatible then
  | Insert into the compatible list
end
end

```

**Algorithm 4:** GetCompatibleRefPatterns

#### 4.3. PerfectMatchRefPattern

The **PerfectMatchRefPattern** method receives as input a list of marked edges and, among all the compatible refinement patterns returned from **GetCompatibleRefPatterns**, finds the patterns that do not refine any edge that is not marked. These are considered to be a *perfectly matched*, meaning that a set of patterns satisfying certain criteria requiring the least amount of refinement has been found. Currently, in the NeoPZ library, the pattern with the least elements in the set of perfect match patterns is chosen.

**PerfectMatchRefPattern** corresponds to the selection of a refinement pattern that creates *transition* refinement patterns to create meshes without hanging nodes.

---

<sup>2</sup>Appropriately permuted as to match node ordering of  $s^i$

#### 4.4. RefineDirectional

Lastly, the **RefineDirectional** method is presented, which has extensive applicability in problems where graded meshes are desired in the direction of a surface, line or point. The idea of refining towards a certain direction has been explored in [18, 25] but limited to simplicial meshes.

The main idea of this method is to refine elements that are neighbors to a given entity (point, line, surface) in such a way that the entity itself is not divided. All the edges that touch the entity and are not included in the entity are divided. The algorithm is described in Algorithm 5.

**RefineDirectional** are illustrated in the examples of Section 6.

```

Input: List of elements that can be refined  $\{K\}$ , identifier  $m$  of the region of interest
for element  $K \in \{K\}$  do
  for vertex  $v$  of  $K$  do
    if  $(K, v)$  has a neighbor with identifier  $m$  then
      | Marked  $v$ 
    end
  end
  if No vertex has been marked then
    | return
  end
  for edge  $e$  of  $K$  do
    if  $(K, e)$  has a neighbor with identifier  $m$  then
      | continue
    end
    if only one vertex  $v_e$  of  $e$  is marked then
      | Mark edge  $e$ 
    end
  end
  Find PerfectMatchRefPattern with marked edges
end

```

**Algorithm 5:** RefineDirectional

## 5. Refinement pattern database

All the operations performed so far depend on the availability of different refinement patterns at runtime. Therefore, one essential part of the usage of refinement patterns is to appropriately store them in a database, which, in the NeopZ library is implemented as a globally accessed instance of the class **TPZRefPatternDataBase**.

The database is populated with refinement patterns that are read from files. When reading a refinement pattern from a file, the **RefPatternEquality** algorithm of Section 4 is used to check if this refinement pattern is already present in the database. If it is not, it is inserted, and indexed by the numerical identifier and name, as shown in Figure 4.

The indexing of the refinement patterns makes searching for a pattern in the database correspond to a map lookup operation, therefore with complexity  $\mathcal{O}(\log n)$ , where  $n$  stands for the number of stored refinement patterns.

For each refinement pattern read from a file, its permutations and side refinement patterns, if not in the database, are added to the database as well.

It is noted that the database also represents a crucial saving of memory for a finite element mesh supporting refinement patterns: each element in the mesh can store a pointer to its refinement pattern, instead of storing the pattern itself. Taking into account that permutations and side refinement patterns are also needed at the element level, it is clear that avoiding duplicate instances of patterns becomes essential when the number of available refinement patterns grows.

All the refinement patterns in the database are available to be used in routines such as **GetCompatibleRefPatterns**, which is called in the operations such as directional refinement (**RefineDirectional**). Therefore, it is important to populate the database with useful patterns. This is done



through a list of patterns stored in text files, which are read before making use of the routines of Section 4.

## 6. Examples

This section is devoted to demonstrating some of the capabilities of the refinement tools that were discussed in the previous sections.

### 6.1. YF-17 aircraft mesh

To illustrate the usage of `RefineDirectional` routine, we consider a surface of a YF-17 fighter jet, available in [26], embedded in a tetrahedral mesh that represents its surrounding air. The initial mesh is shown in Figure 5, and consists of 359 696 tetrahedral elements.

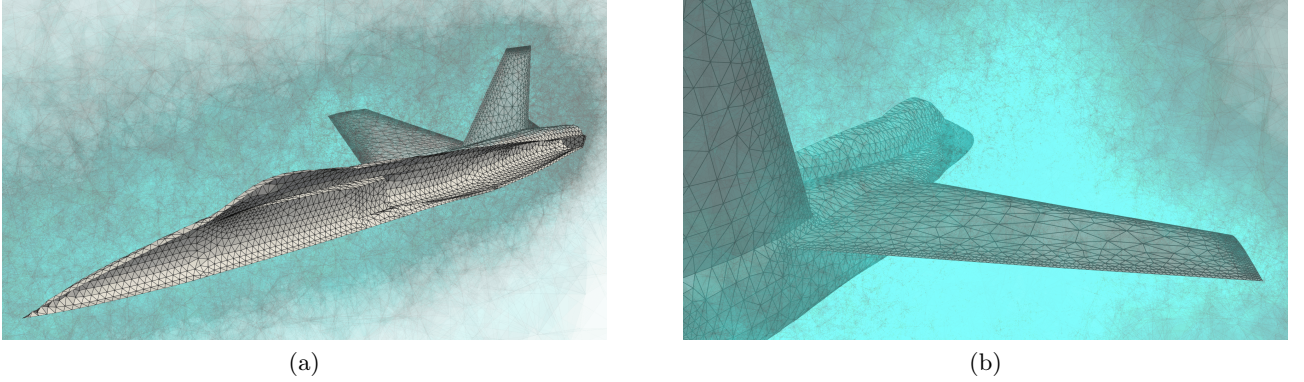


Figure 5: YF-17 aircraft mesh. (a) Perspective view and (b) rear view.

In order to accurately capture the boundary layer effects of the airflow near the aircraft surface, a finer mesh is usually needed in that region. The directional refinement tool is tailored for this kind of problem, as it allows the user to refine elements that are neighbors to a given geometrical entity, such as a point, a curve or a surface. We apply five consecutive refinements, leading to the mesh layers displayed in Figures 6-7.

In Figure 8, it can be observed that the aircraft surface mesh is not modified as new layers of elements are introduced in the 3D domain surrounding the surface. As stated in Section 3.2, the refinement at the element level occurs following a predefined pattern stored in a database. For tetrahedra, the pattern that matches the desired refinement strategy will not always produce child elements whose topology is the same as the parent element. To better exemplify this, figures 9-10 depict two tetrahedral elements that share a line and a facet, respectively, with the aircraft surface. In the first case, the first level of refinement leads to two child elements with wedge topology, while in the second case, the tetrahedron is split into a smaller tetrahedron and a wedge. During the third and fourth refinement steps, some hexahedral elements are created when the father element is refined towards a line, while for the facet case, the remaining refinements produce only wedge elements.

### 6.2. Fracture propagation

Hydraulic fracturing is a common procedure used in the oil industry to enhance the rates of injection and production of a wellbore. In this process, a fracture is propagated through the injection of pressurized fluid through the wellbore. This procedure is illustrated for the case of a vertical wellbore in Figure 11, where two vertical fractures are propagated perpendicular to the minimum in-situ stress direction. Several methodologies have been proposed to simulate this process within the context of the Finite Element Method [27–36]. One possibility to increase efficiency is to only model one-fourth of the domain as shown in Figure 12.

The basis of this problem is to define a line that represents the geometry of the fracture. This line intersects the 3D elements of the domain, and the refinement patterns are used to create a mesh conforming to this line as shown in Figure 13.

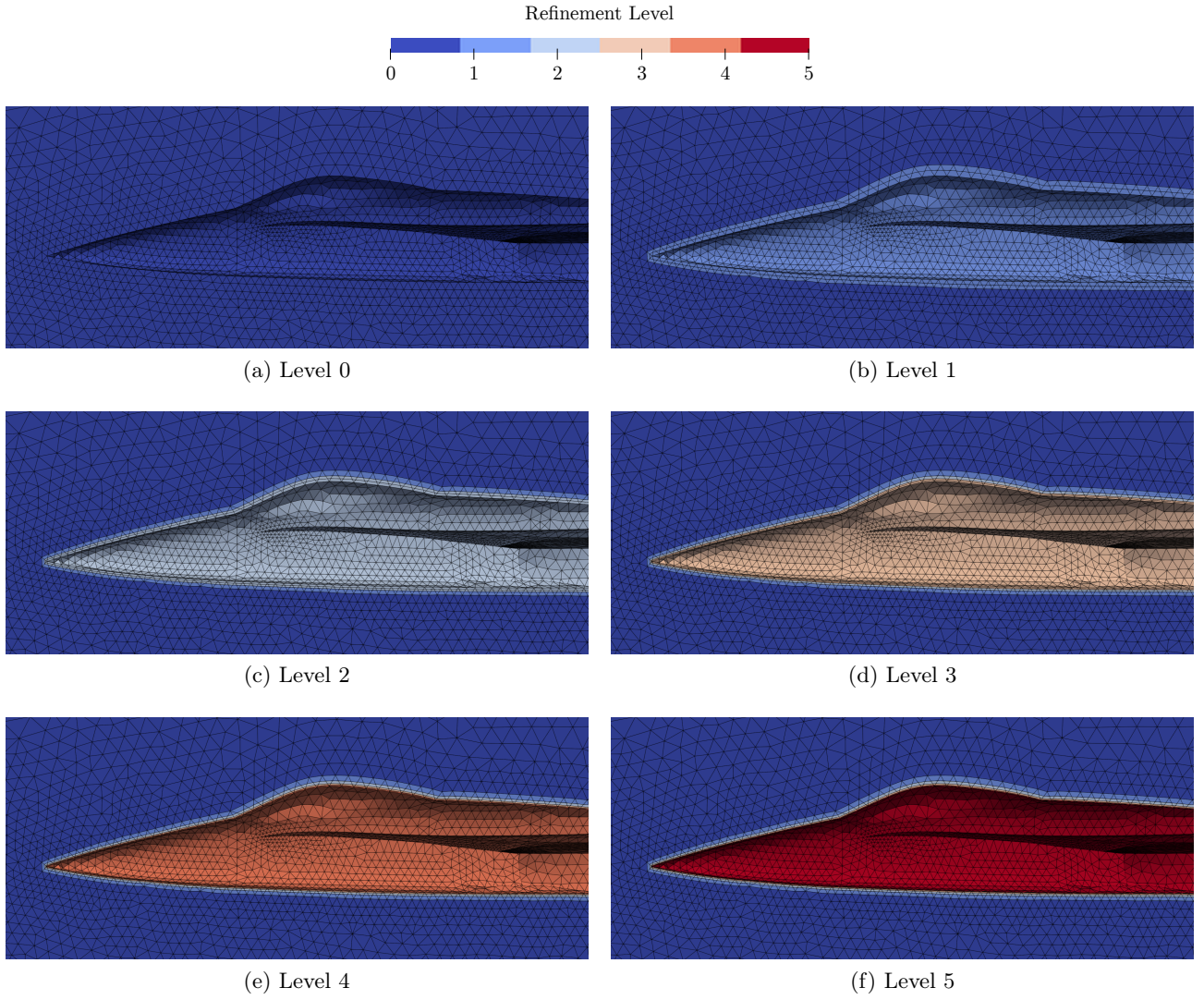


Figure 6: YF-17 aircraft mesh. Lateral view of five levels of directional refinements.

It is well known that this kind of problem presents a singular stress field in the vicinity of the crack contour, so one possible strategy to tackle this issue is to refine the mesh near this region in order to better capture this stress concentration. To avoid global mesh refinement and improve the computational efficiency, one directional mesh refinement step is applied towards the fracture contour, as shown in Figure 14.

### 6.3. A structural casket designed to run experiments of petroleum engineering

This example is based on a real prototype being developed at Unicamp. It consists of a structural module made of steel, designed to withstand a uniform pressure load on its inner surface. The geometry and boundary conditions lead to an axisymmetric problem, so for simplicity, only half of the casket is modeled according to Figure 15. Stiffeners are placed on the upper and lower flanges to prevent buckling and increase local stability. However, the presence of these stiffeners induces a stress concentration that needs to be accurately captured by the numerical simulation. When using FEM formulations, a major concern is the mesh quality in this region which generally needs to be more refined than the rest of the domain.

One option to tackle this problem is to adopt 1-irregular meshes and perform adaptive refinements toward the regions of interest. However, this strategy may lead to a high computational cost, as the number of degrees of freedom increases significantly. Alternatively, the directional refinement tool can be used to refine the mesh towards the stiffener line shown in Figure 15b. In Figure 16, three steps of directional refinement are applied towards these lines, showing elements with good aspect ratio while creating graded elements in the direction of the region of interest.

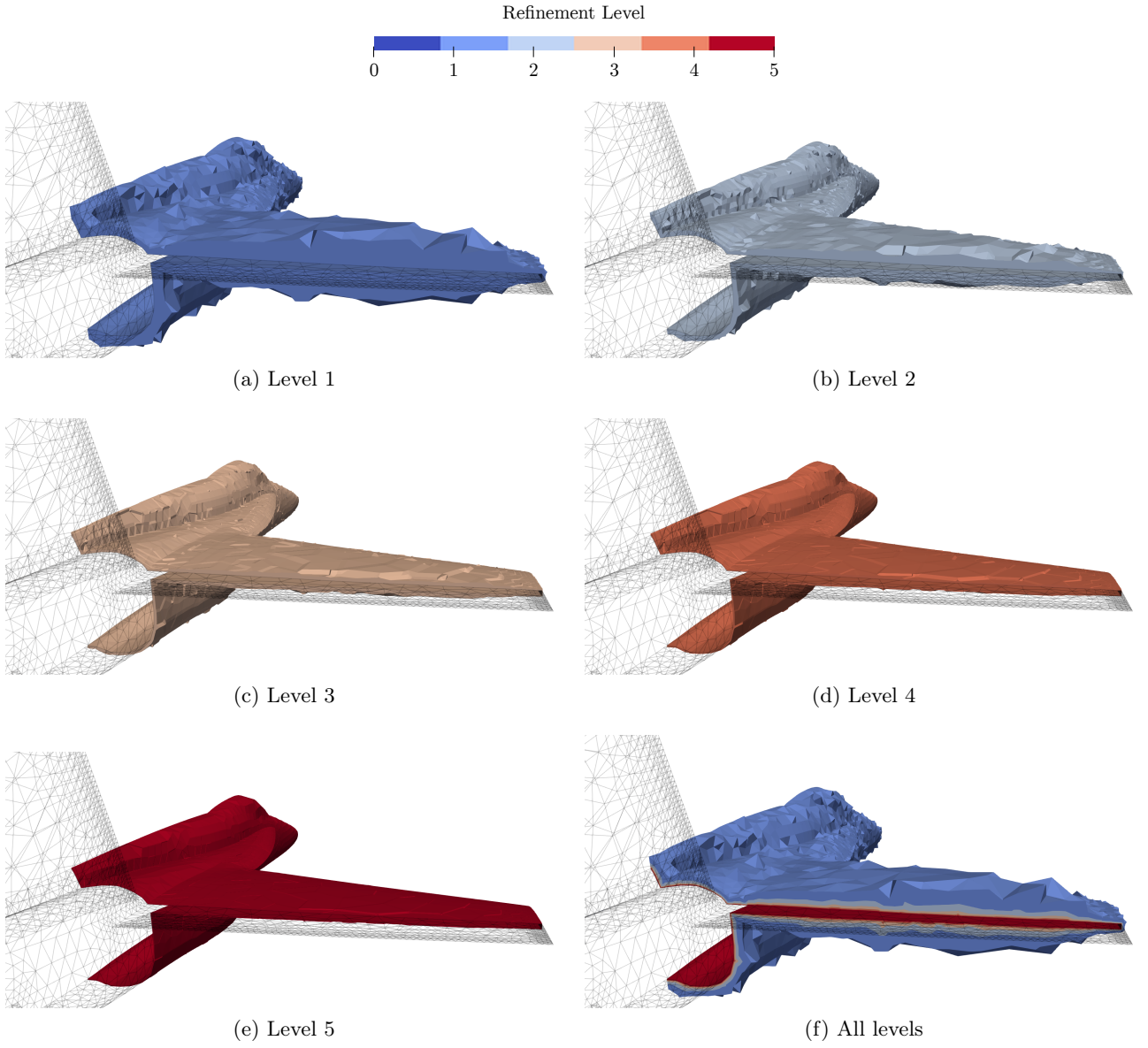


Figure 7: YF-17 aircraft mesh. Rear view of five levels of directional refinements.

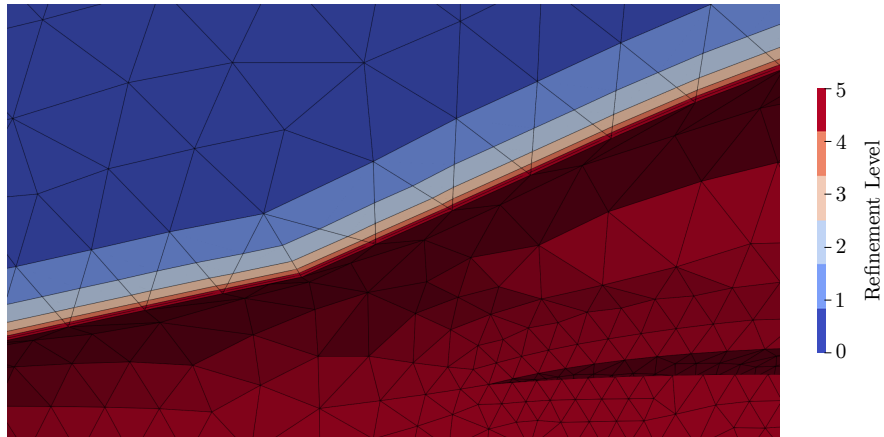


Figure 8: YF-17 aircraft mesh. Boundary layers after five levels of refinements.

#### 6.4. 1-irregular and directional refinement of a cross-shaped geometry

In fluid dynamics, the presence of a no-slip boundary condition (zero tangential velocity), often results in a *boundary layer* scenario, in which the solution field presents a strong gradient towards the normal direction of the boundary of the domain. To analyze the applicability of the refinement



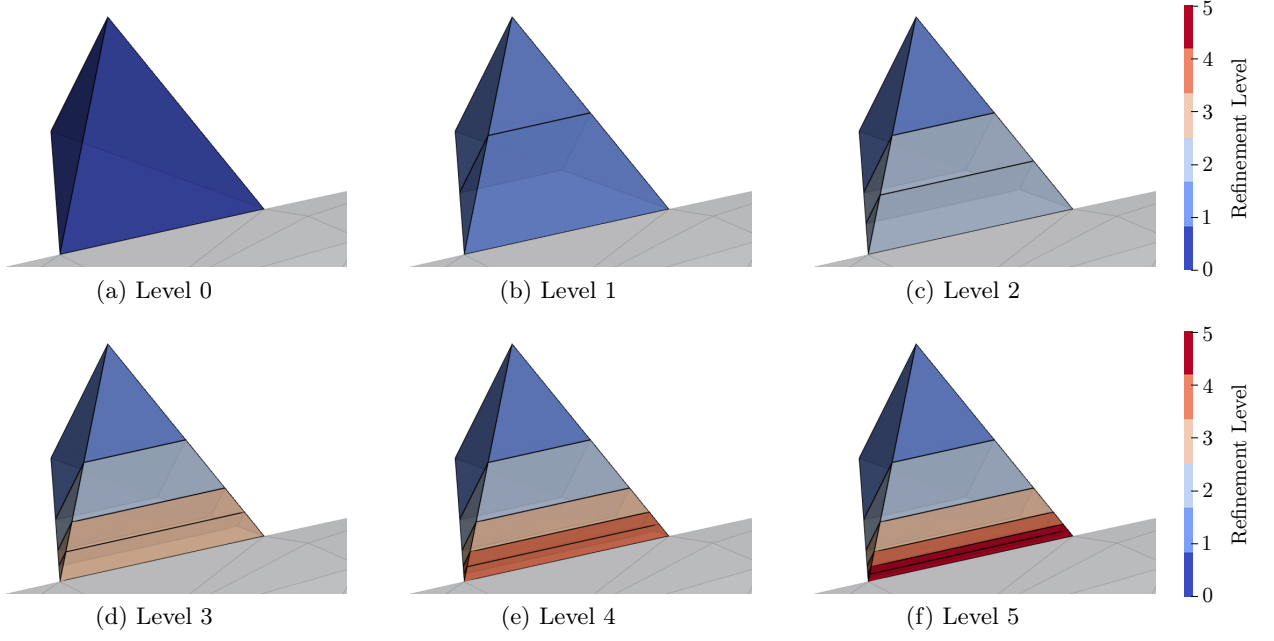


Figure 9: YF-17 aircraft mesh. Successive refinements over an element that shares a line with the aircraft surface.

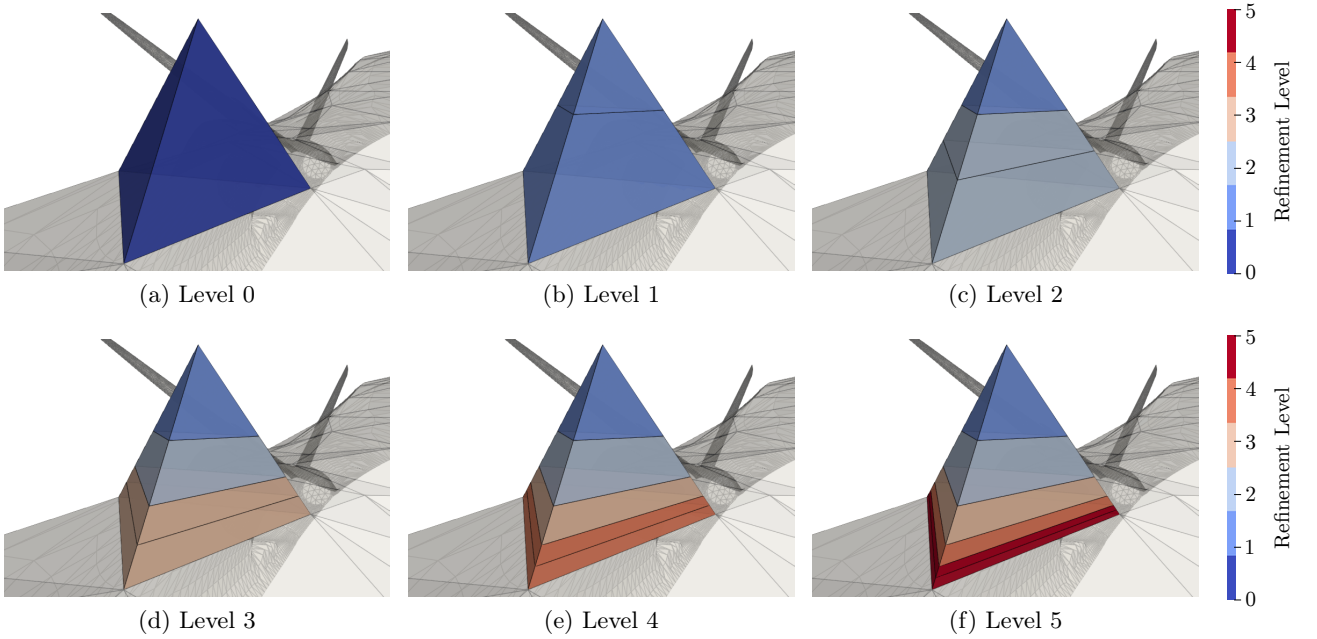


Figure 10: YF-17 aircraft mesh. Successive refinements over an element that shares a facet with the aircraft surface.

patterns in such scenarios, Figure 17 illustrates a cross-shaped geometry divided into two subregions denoted by  $\Omega_0$  and  $\Omega_1$ , whose boundaries are named  $\Gamma_0$  and  $\Gamma_1$ , respectively. For each subregion, a refinement strategy towards the boundary is applied. The elements of  $\Omega_0$  are refined uniformly, *i.e.*, using a refinement pattern in which the aspect ratio of the refined elements is similar to the original one. In  $\Omega_1$ , however, the **RefineDirectional** algorithm is applied. An unstructured mesh composed of triangular elements is adopted as an initial mesh for both subregions, as shown in Figure 17b.

The different refinement strategies are performed in each subregion in three subsequent levels. For each level, neighboring elements to the boundary are refined using the pattern adopted for that subregion. Figure 18 shows the resulting mesh at each level of refinement.

The refinement strategy applied in  $\Omega_1$  results in a significantly smaller number of elements, while retaining a similar element size in the normal direction to the boundary. Therefore, in a boundary-layer situation, this mesh is expected to be able to represent the gradients of the solution with better

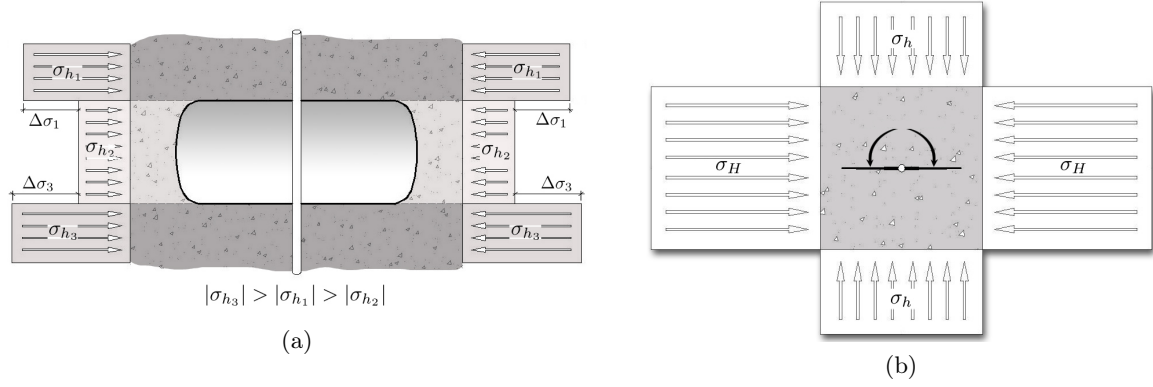


Figure 11: Illustration of hydraulic fracture propagation. (a) Side view and (b) top view with arrows indicating the 2 fractures being propagated from the wellbore.

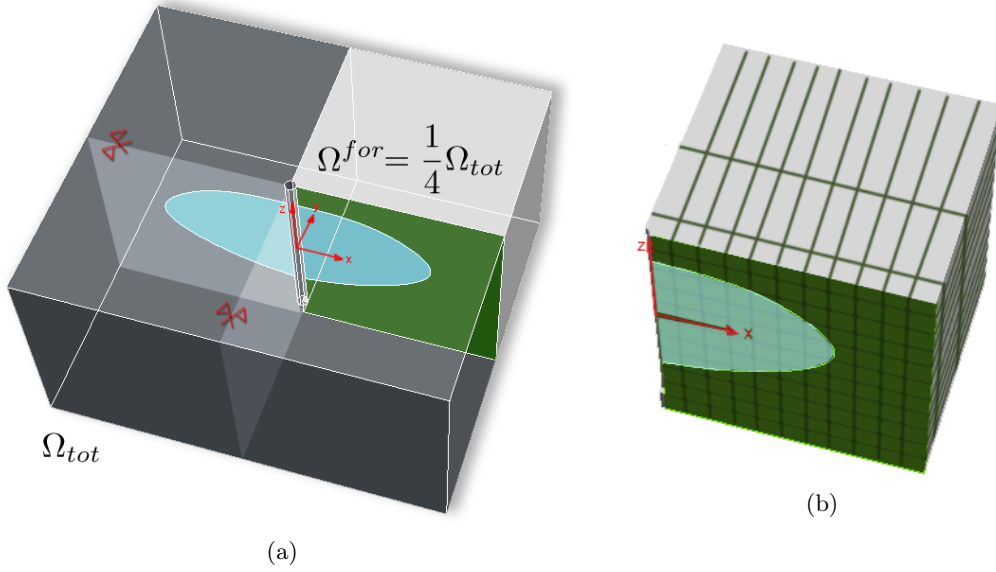


Figure 12: Illustration of the simulation domain used within the context of the FEM. (a) Complete domain and (b) one-fourth of the domain used for the simulation.

efficiency than with the uniform refinement strategy adopted in  $\Omega_0$ .

## 7. Conclusions

A methodology for generalizing h adaptivity in the context of Finite Element meshes is presented and the concept of refinement patterns is introduced. A refinement pattern is defined as an arbitrary partition of a master element. In order to describe refinement patterns formally, each master element is identified as the union of its sides. Each side of a sub-element is necessarily contained in a side of its father element, and an affine transformation allows to map points between sides.

The refinement patterns documented in this work and their management in a database offer its users a toolset to refine a mesh in an innovative way. This is exemplified by the use of directional refinements which can be applied to a variety of problems where the solution field presents strong gradients in a specific direction. The effectiveness of the refinement patterns is demonstrated through specialized mesh refinements applied to problems with complex geometries. The methodology is implemented in the NeoPZ library, and the results obtained in the examples presented in this chapter show the potential of the proposed approach in improving the efficiency of finite element simulations.

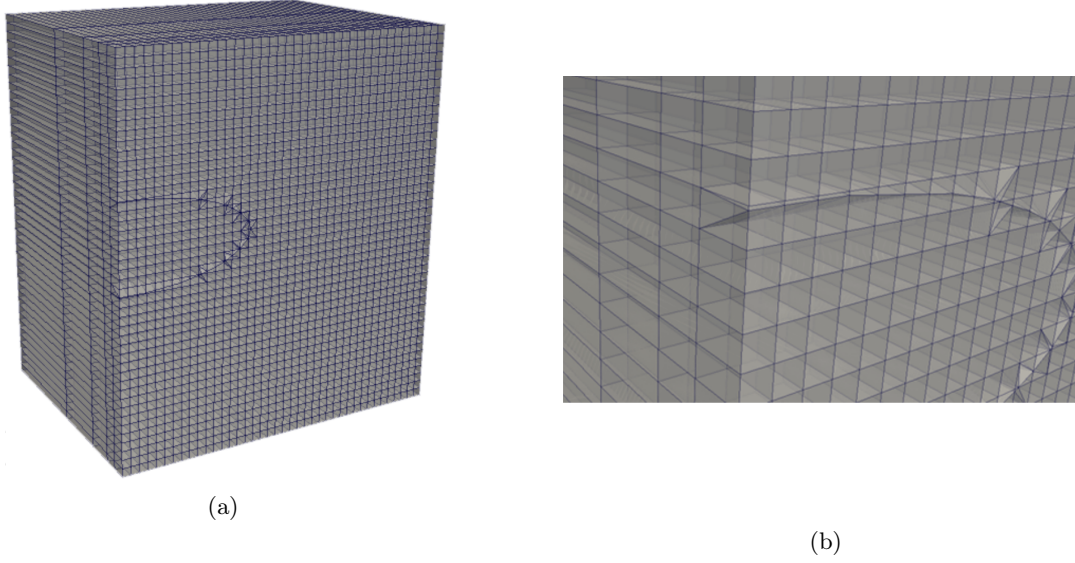


Figure 13: Rock matrix with a vertical fracture. (a) Initial mesh and (b) fracture detail.

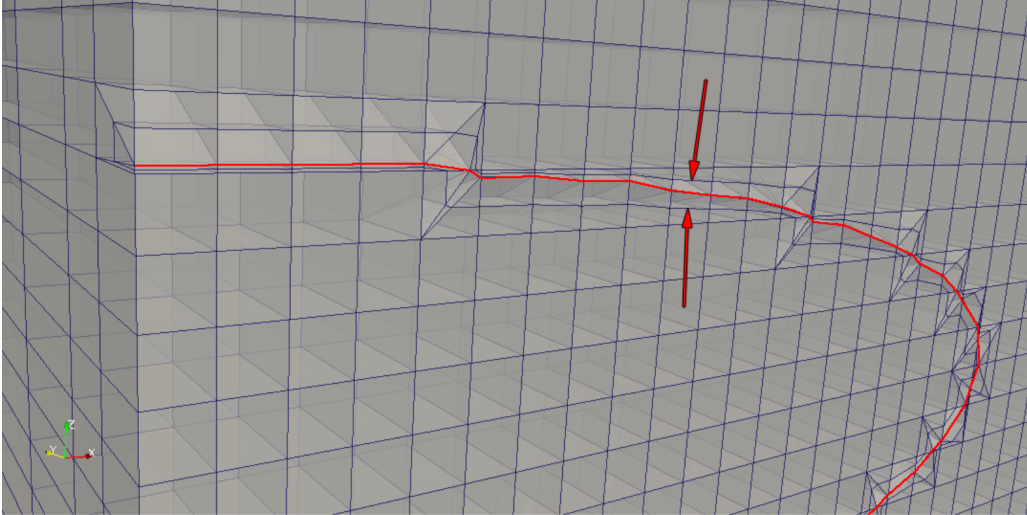


Figure 14: Rock matrix with a vertical fracture. Refinement towards the fracture contour.

## 8. Extensions and future work

The methodology presented in this work is a first step towards the development of a general framework for mesh adaptivity. Refinement patterns at this point assume fixed positions of the nodes in the master element. A natural extension of this work is to allow for the movement of nodes in the master element. This would allow for the creation of more general refinement patterns, leading to arbitrarily graded meshes.

It should also be noted that the methodology can be applied to higher-dimension meshes, generalizing the concept h-refinement.

**Acknowledgments:** The authors gratefully acknowledge the support of ANP - *Brazil's National Oil, Natural Gas and Biofuels Agency* through the R&D levy regulation and TotalEnergies through research project 5955 with Unicamp. The authors also acknowledge the support of EPIC – *Energy Production Innovation Center*, hosted by the University of Campinas (UNICAMP) and sponsored by Equinor Brazil and FAPESP – *São Paulo Research Foundation* (2017/15736-3). Acknowledgments are extended to the Center for Petroleum Studies (CEPETRO) and the School of Civil Engineering, Architecture and Urban Planning (FECFAU). Author G. Avancini gratefully acknowledges Equinor/FAPESP and

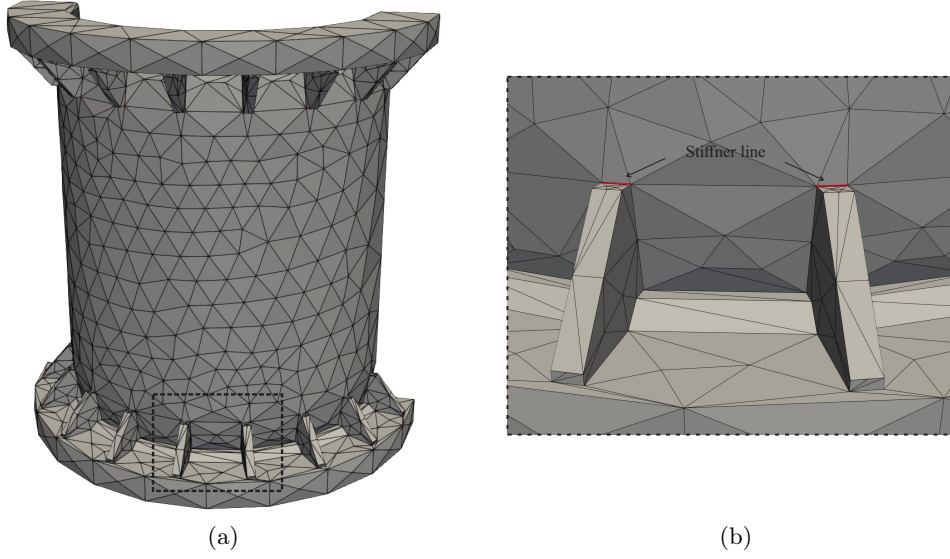


Figure 15: Structural casket. (a) Initial mesh and (b) detail of the stiffeners.

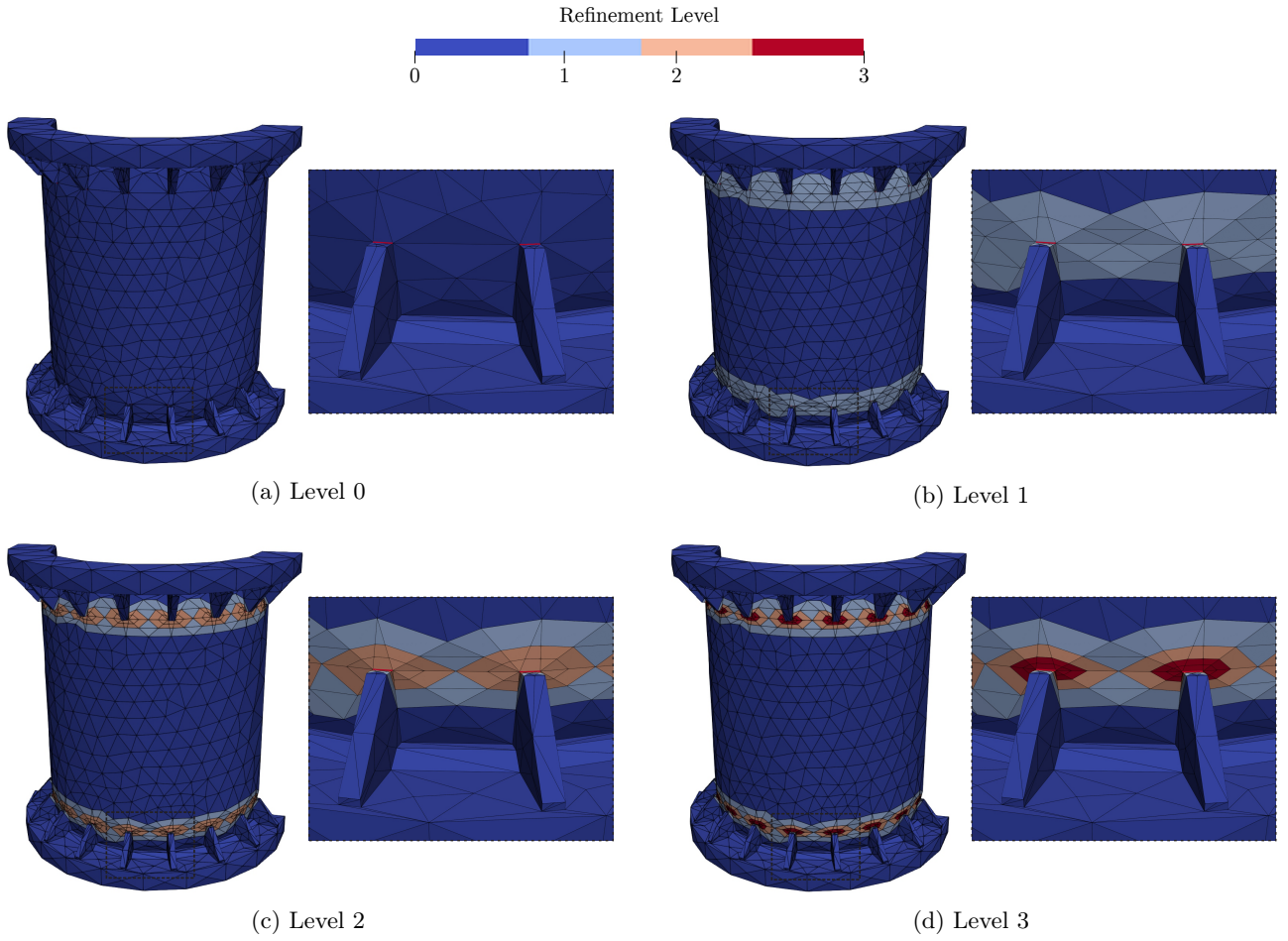


Figure 16: Structural casket. Successive refinements towards the stiffeners

TotalEnergies/FUNCAMP for the financial support (grants 2023/06981-5 and 76042-23). Authors P. R. B. Devloo (grants 305823/2017-5 and 309597/2021-8) and F. T. Orlandini (grant 130002/2022-7) thankfully acknowledges financial support from the CNPq - *Conselho Nacional de Desenvolvimento Científico e Tecnológico*.



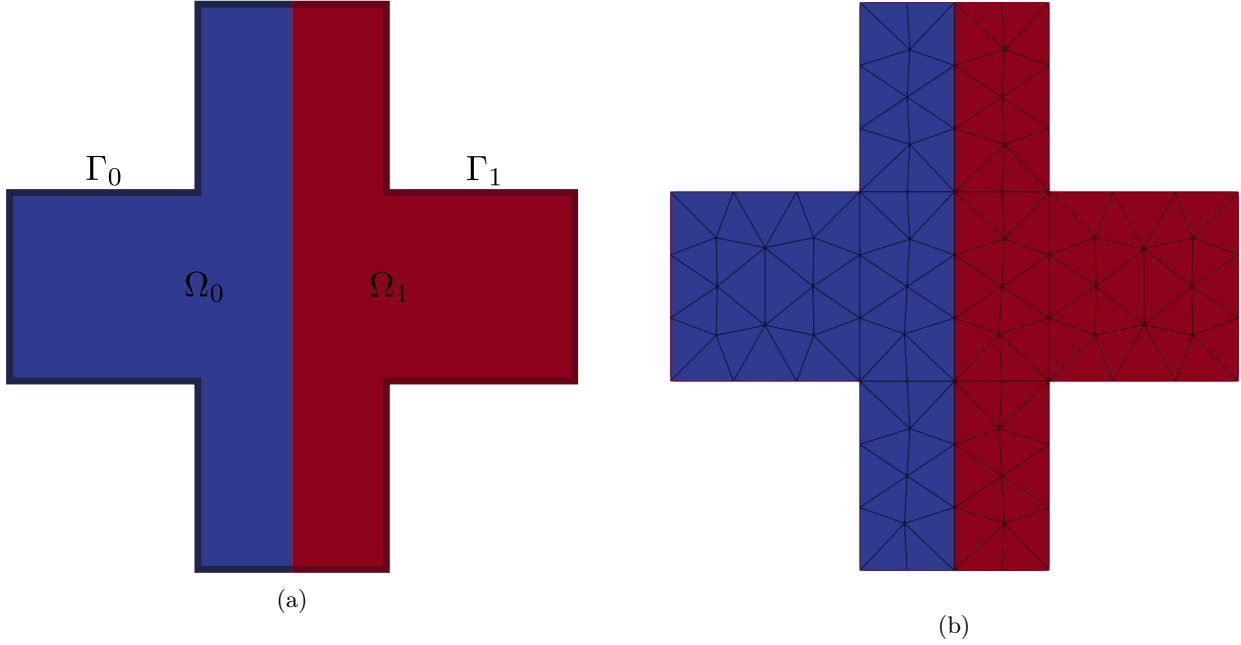
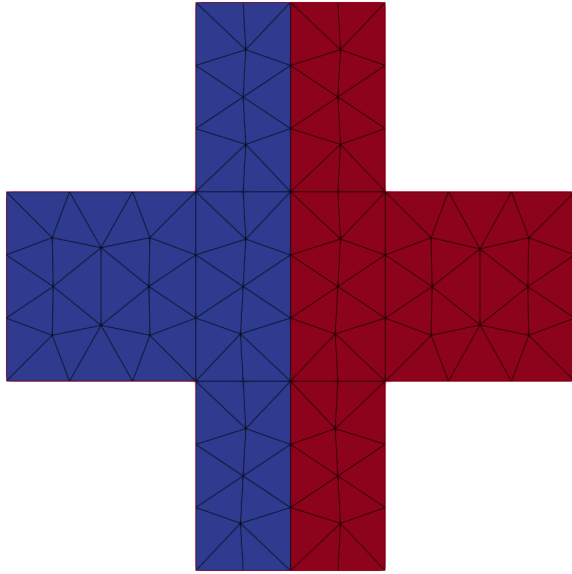


Figure 17: Cross-shaped geometry. (a) subregions and boundary details and (b) initial triangular mesh

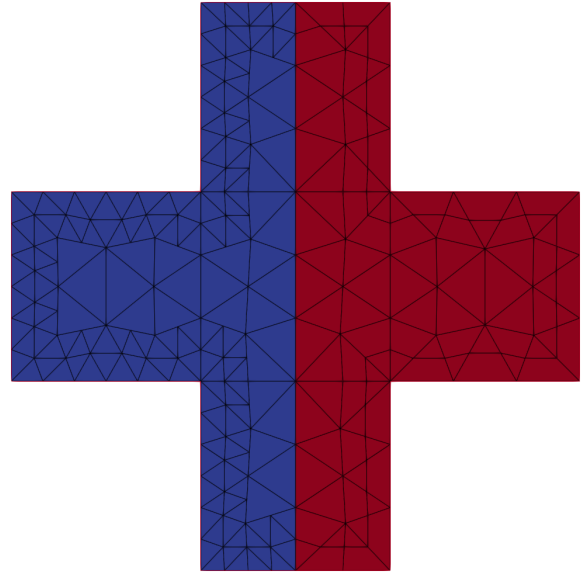
## References

- [1] I. Babuška, The p and h-p versions of the finite element method: The state of the art, in: D. L. Dwoyer, M. Y. Hussaini, R. G. Voigt (Eds.), *Finite Elements*, Springer New York, New York, NY, 1988, pp. 199–239.
- [2] I. Babuska, M. Suri, The p and h-p versions of the finite element method, basic principles and properties, *SIAM Review* 36 (4) (1994) 578–632.
- [3] L. Demkowicz, W. Rachowicz, P. Devloo, A Fully Automatic hp-Adaptivity, *Journal of Scientific Computing* 17 (1) (2002) 117–142. doi:<https://doi.org/10.1023/A:1015192312705>.
- [4] W. Gui, I. Babuška, The h, p and h-p Versions of the Finite Element Method in 1 Dimension, *Numerische Mathematik* 49 (6) (1986) 613–657. doi:[10.1007/BF01389734](https://doi.org/10.1007/BF01389734).
- [5] L. Demkowicz, P. Devloo, J. Oden, On an h-type mesh-refinement strategy based on minimization of interpolation errors, *Computer Methods in Applied Mechanics and Engineering* 53 (1) (1985) 67–89. doi:[https://doi.org/10.1016/0045-7825\(85\)90076-3](https://doi.org/10.1016/0045-7825(85)90076-3).
- [6] J. Oden, T. Strouboulis, P. Devloo, Adaptive finite element methods for the analysis of inviscid compressible flow: Part i. fast refinement/unrefinement and moving mesh methods for unstructured meshes, *Computer Methods in Applied Mechanics and Engineering* 59 (3) (1986) 327–362. doi:[https://doi.org/10.1016/0045-7825\(86\)90004-6](https://doi.org/10.1016/0045-7825(86)90004-6).
- [7] P. Devloo, J. Tinsley Oden, P. Pattani, An h-p adaptive finite element method for the numerical simulation of compressible flow, *Computer Methods in Applied Mechanics and Engineering* 70 (2) (1988) 203–235. doi:[https://doi.org/10.1016/0045-7825\(88\)90158-2](https://doi.org/10.1016/0045-7825(88)90158-2).
- [8] P. Devloo, J. Oden, T. Strouboulis, Implementation of an adaptive refinement technique for the supg algorithm, *Computer Methods in Applied Mechanics and Engineering* 61 (3) (1987) 339–358. doi:[https://doi.org/10.1016/0045-7825\(87\)90099-5](https://doi.org/10.1016/0045-7825(87)90099-5).
- [9] P. R. B. Devloo, PZ: An object oriented environment for scientific programming, *Computer Methods in Applied Mechanics and Engineering* 150 (1-4) (1997) 133–153. doi:[10.1016/S0045-7825\(97\)00097-2](https://doi.org/10.1016/S0045-7825(97)00097-2).
- [10] D. J. Morton, J. M. Tyler, J. R. Dorroh, A new 3d finite element for adaptive h-refinement in 1-irregular meshes, *International Journal for Numerical Methods in Engineering* 38 (23) (1995) 3989–4008. doi:<https://doi.org/10.1002/nme.1620382306>.
- [11] P. Di Stolfo, A. Schröder, N. Zander, S. Kollmannsberger, An easy treatment of hanging nodes in hp-finite elements, *Finite Elements in Analysis and Design* 121 (2016) 101–117. doi:<https://doi.org/10.1016/j.finel.2016.07.001>.
- [12] T.-P. Fries, A. Byfut, A. Alizada, K. W. Cheng, A. Schröder, Hanging nodes and xfem, *International Journal for Numerical Methods in Engineering* 86 (4-5) (2011) 404–430. doi:<https://doi.org/10.1002/nme.3024>.
- [13] S. Huo, G. Liu, J. Zhang, C. Song, A smoothed finite element method for octree-based polyhedral meshes with large number of hanging nodes and irregular elements, *Computer Methods in Applied Mechanics and Engineering* 359 (2020) 112646. doi:<https://doi.org/10.1016/j.cma.2019.112646>.
- [14] Y. jie Huang, Z. jun Yang, H. Zhang, S. Natarajan, A phase-field cohesive zone model integrated with cell-based smoothed finite element method for quasi-brittle fracture simulations of concrete at mesoscale, *Computer Methods in Applied Mechanics and Engineering* 396 (2022) 115074. doi:<https://doi.org/10.1016/j.cma.2022.115074>.
- [15] E. Aulisa, G. Capodaglio, G. Ke, Construction of h-refined continuous finite element spaces with arbitrary hanging

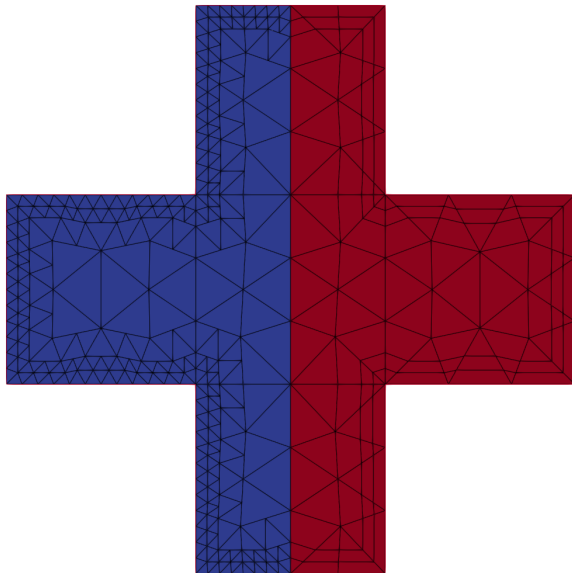




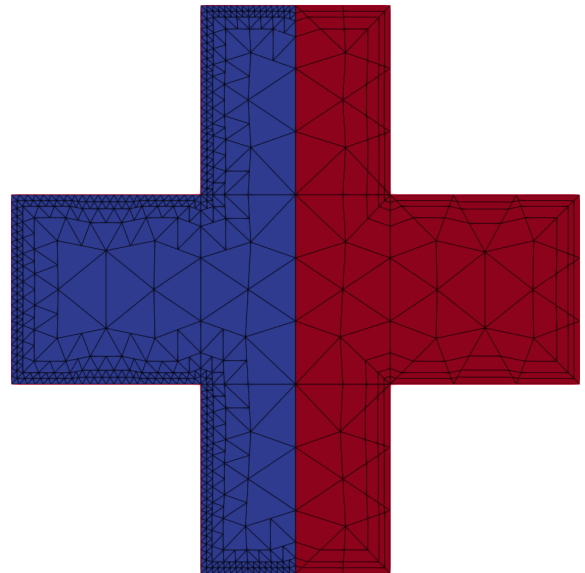
(a) Level 0



(b) Level 1



(c) Level 2



(d) Level 3

Figure 18: Cross-shaped geometry. Sequence of refinements in both  $\Omega_0$  and  $\Omega_1$ .

node configurations and applications to multigrid algorithms, SIAM Journal on Scientific Computing 41 (1) (2019) A480–A507. doi:[10.1137/18M1175409](https://doi.org/10.1137/18M1175409).

- [16] O. C. Zienkiewicz, J. Z. Zhu, N. G. Gong, Effective and practical h-p-version adaptive analysis procedures for the finite element method, International Journal for Numerical Methods in Engineering 28 (4) (1989) 879–891. doi:<https://doi.org/10.1002/nme.1620280411>.
- [17] M. C. Rivara, Algorithms for refining triangular grids suitable for adaptive and multigrid techniques, International Journal for Numerical Methods in Engineering 20 (4) (1984) 745–756. doi:<https://doi.org/10.1002/nme.1620200412>.
- [18] M.-C. Rivara, Mesh refinement processes based on the generalized bisection of simplices, SIAM Journal on Numerical Analysis 21 (3) (1984) 604–613. doi:[10.1137/0721042](https://doi.org/10.1137/0721042).
- [19] M.-C. Rivara, C. Levin, A 3-d refinement algorithm suitable for adaptive and multi-grid techniques, Communications in Applied Numerical Methods 8 (5) (1992) 281–290. doi:<https://doi.org/10.1002/cnm.1630080502>.
- [20] X. Zhao, S. Mao, Z. Shi, Adaptive finite element methods on quadrilateral meshes without hanging nodes, SIAM Journal on Scientific Computing 32 (4) (2010) 2099–2120. doi:<https://doi.org/10.1137/090772022>.
- [21] F. Jaillet, C. Lobos, Fast Quadtree/Octree adaptive meshing and re-meshing with linear mixed elements, Engineering

- with Computers 38 (4) (2022) 3399–3416. doi:<https://doi.org/10.1007/s00366-021-01330-w>.
- [22] G. Avancini, N. Shauer, F. T. Orlandini, P. C. A. Lucci, P. R. B. Devloo, Extending h adaptivity with refinement patterns, in: *Advances in Applied Mechanics*, Vol. 59, Error control, adaptive discretizations and applications, Elsevier, *forthcoming*, Ch. 30, Part 2.
  - [23] Wikipedia, [Graphics processing unit — Wikipedia, the free encyclopedia](https://en.wikipedia.org/wiki/Graphics_processing_unit), [Online; accessed 28-March-2024] (2024). URL [https://en.wikipedia.org/wiki/Graphics\\_processing\\_unit](https://en.wikipedia.org/wiki/Graphics_processing_unit)
  - [24] P. R. B. Devloo, C. M. A. Ayala Bravo, E. C. Rylo, Systematic and generic construction of shape functions for p-adaptive meshes of multidimensional finite elements, *Computer Methods in Applied Mechanics and Engineering* 198 (21) (2009) 1716–1725. doi:<https://doi.org/10.1016/j.cma.2008.12.022>.
  - [25] O. C. Zienkiewicz, J. Wu, Automatic directional refinement in adaptive analysis of compressible flows, *International Journal for Numerical Methods in Engineering* 37 (13) (1994) 2189–2210. doi:<https://doi.org/10.1002/nme.1620371304>.
  - [26] Unstructured mesh for YF-17 with solution, <https://cgns.github.io/CGNSFiles.html>, accessed: 2024-02-15.
  - [27] N. Shauer, C. Duarte, Improved algorithms for generalized finite element simulations of three-dimensional hydraulic fracture propagation, *International Journal for Numerical and Analytical Methods in Geomechanics* 43 (18) (2019) 2707–2742. doi:<https://doi.org/10.1002/nag.2977>.
  - [28] N. Shauer, C. Duarte, A generalized finite element method for three-dimensional hydraulic fracture propagation: Comparison with experiments, *Engineering Fracture Mechanics* 235 (2020) 107098. doi:<https://doi.org/10.1016/j.engfracmech.2020.107098>.
  - [29] N. Shauer, C. Duarte, A three-dimensional generalized finite element method for simultaneous propagation of multiple hydraulic fractures from a wellbore, *Engineering Fracture Mechanics* 265 (2022) 108360. doi:<https://doi.org/10.1016/j.engfracmech.2022.108360>.
  - [30] P. R. Devloo, P. D. Fernandes, S. M. Gomes, C. M. A. A. Bravo, R. G. Damas, A finite element model for three dimensional hydraulic fracturing, *Mathematics and Computers in Simulation* 73 (1) (2006) 142–155. doi:<https://doi.org/10.1016/j.matcom.2006.06.020>.
  - [31] J. Adachi, E. Siebrits, A. Peirce, J. Desroches, Computer simulation of hydraulic fractures, *International Journal of Rock Mechanics & Mining Sciences* 44 (2007) 739–757. doi:[10.1016/j.ijrmms.2006.11.006](https://doi.org/10.1016/j.ijrmms.2006.11.006).
  - [32] B. Lecampion, A. Bunger, X. Zhang, Numerical methods for hydraulic fracture propagation: A review of recent trends, *Journal of Natural Gas Science and Engineering* 49 (2018) 66–83. doi:[10.1016/j.jngse.2017.10.012](https://doi.org/10.1016/j.jngse.2017.10.012).
  - [33] S. T. Castonguay, M. E. Mear, R. H. Dean, J. H. Schmidt, Predictions of the growth of multiple interacting hydraulic fractures in three dimensions, in: *Proceedings of SPE Annual Technical Conference and Exhibition*, Society of Petroleum Engineers, New Orleans, LA, USA, 2013, p. 12. doi:[10.2118/166259-MS](https://doi.org/10.2118/166259-MS).
  - [34] S. Salimzadeh, T. Usui, A. Paluszny, R. W. Zimmerman, Finite element simulations of interactions between multiple hydraulic fractures in a poroelastic rock, *International Journal of Rock Mechanics and Mining Sciences* 99 (2017) 9 – 20. doi:[10.1016/j.ijrmms.2017.09.001](https://doi.org/10.1016/j.ijrmms.2017.09.001).
  - [35] K. Wu, J. E. Olson, M. T. Balhoff, W. Yu, Numerical analysis for promoting uniform development of simultaneous multiple-fracture propagation in horizontal wells, *SPE Production & Operations* 32 (01) (2017) 41–50. doi:[10.2118/174869-PA](https://doi.org/10.2118/174869-PA).
  - [36] L.-P. Yi, X.-G. Li, Z.-Z. Yang, H. Waisman, A fully coupled fluid flow and rock damage model for hydraulic fracture of porous media, *Journal of Petroleum Science and Engineering* 178 (2019) 814 – 828. doi:<https://doi.org/10.1016/j.petrol.2019.03.089>.